Nonequilibrium phonon effects on electron transport in GaAs-based mid-infrared quantum cascade lasers

Y. B. Shi and I. Knezevic
Department of Electrical and Computer Engineering, University of Wisconsin - Madison
1415 Engineering Dr, Madison, WI 53706-1691, USA
Email: yshi9@wisc.edu, knezevic@engr.wisc.edu

INTRODUCTION

The dominant energy relaxation mechanism of electrons in quantum cascade lasers (QCLs) is the non-radiative scattering with optical phonons [1]. Through optical phonon emissions, the injected electrons in the upper lasing level are rapidly transferred to the lower lasing level, and the carrier life time in the upper lasing subband is significantly reduced. Consequently, a large current must be supplied in order to create sufficient population inversion and to achieve the lasing condition, which limits the efficiency of the laser. The impact of out-of-equilibrium phonons in terahertz QCLs has been investigated both experimentally [2] and theoretically [3], [4].

In this paper, we present an ensemble Monte Carlo (EMC) simulation describing the dynamics of the interacting electron and phonon systems in GaAs-based mid-infrared QCLs.

THEORY

Within the semiclassical framework, the dynamics of the electron-phonon interacting system in QCLs can be described by the coupled Boltzmann equations [3]:

$$\frac{\partial f_{\mathbf{k}_\parallel,i}}{\partial t} = \left.\frac{\partial f_{\mathbf{k}_\parallel,i}}{\partial t}\right|_{e-ph} + \left.\frac{\partial f_{\mathbf{k}_\parallel,i}}{\partial t}\right|_{e-e}, \quad (1)$$

$$\frac{\partial N_{\mathbf{q}}}{\partial t} = \left.\frac{\partial N_{\mathbf{q}}}{\partial t}\right|_{ph-e} + \left.\frac{\partial N_{\mathbf{q}}}{\partial t}\right|_{ph-ph}, \quad (2)$$

where $f_{\mathbf{k}_\parallel,i}$ is the electron distribution function in subband i with in-plane wave vector $\mathbf{k}_\parallel$, and $N_{\mathbf{q}}$ is the optical phonon distribution with wave vector $\mathbf{q}$. The two kinetic equations are coupled through the electron-phonon collision integrals $\left(\partial f_{\mathbf{k}_\parallel,i}/\partial t\right)\big|_{e-ph}$ and $\left(\partial N_{\mathbf{q}}/\partial t\right)\big|_{ph-e}$, which can be evaluated using Fermi's Golden Rule. The phonon equation can be simplified by applying the relaxation time approximation on the phonon-phonon interaction term:

$$\left.\frac{\partial N_{\mathbf{q}}}{\partial t}\right|_{ph-ph} = -\frac{N_{\mathbf{q}} - N_0}{\tau_{op}(T_L)}, \quad (3)$$

where N_0 is the thermal equilibrium phonon number, and τ_{op} is the lattice temperature-dependent phonon relaxation time describing the anharmonic decay process of LO phonons. The dominant anharmonic decay mechanism for LO phonons is the decay into two LA phonons with equal energies and opposite momenta. Based on this approximation, τ_{op} can be analytically derived [5].

A particle-based EMC approach is developed to solve the coupled kinetic equations for QCLs. The electron transport is determined by the scattering between subbands, and both electron–LO phonon and electron–electron scattering mechanisms are taken into account. In order to properly describe the phonon evolution, Eq. (3), a phonon distribution histogram over a grid in $\mathbf{q}$-space is set up to keep track of the number of nonequilibrium "numerical" phonons [3]. The LO phonon distribution is assumed isotropic in plane due to the lack of electrical field along this direction. The cross-plane distribution is determined by the overlap integral of the initial and final states involved in the interaction. The histogram is updated in each time step as soon as an electron–LO phonon scattering event happens. At the end of the time step, the remaining nonequilibrium LO phonons are allowed to randomly decay into acoustic phonons based on the temperature-dependent average decay time $\tau_{op}(T_L)$.

NUMERICAL RESULTS

The simulated device is a GaAs-based mid-infrared QCL designed for emission at 9.4 μm [6]. Figure 1 shows the subband energy levels and wavefunction moduli squared in two stages under 53 kV/cm (above the threshold) and at 77 K. The three red (bold) curves (from top to bottom) represent the upper and lower lasing levels and the ground state in the active region, while the blue (normal) and green (dashed) curves represent the injector states and the Γ continuum states, respectively. The phonon distribution extracted from the simulation is shown in Fig. 2. The distribution has a peak close to the zone center, which implies that majority of generated phonons have small q. This feature can be explained by the phonon emission rate decaying as a function of $1/q^2$. Figure 3 shows the time evolution of the electron density in three states in the active region with equilibrium (normal) and nonequilibrium (bold) phonons. The excess phonons enhance the phonon absorption rate and enable more electrons from the ground state in the active region and the injector states in the next stage to transfer to the lower lasing level (thermal backfilling). On the other hand, the enhanced phonon absorption also leads to more electrons in the upper lasing level gaining energy and leaking to Γ continuum states or the injector states of the previous stage. The overall effect is reducing the population inversion (the difference of electron density between upper and lower lasing level) and thus degrades performance. The

ISBN 978-2-9547858-0-6

simulated current-field characteristics at 77 K and 300 K with equilibrium and nonequilibrium phonons are shown in Fig. 4. The nonequilibrium phonon effect on current is more obvious at low temperatures when the thermal phonon number is negligibly small.

Conclusion

We present an EMC-based simulation to self-consistently solve the coupled electron and phonon transport equations. The nonequilibrium phonon effects in a GaAs-based mid-infrared QCL were investigated. The results show that the nonequilibrium phonons reduce the population inversion by increasing thermal backfilling and have a larger impact on current density at low temperatures.

Acknowledgment

This work was supported by the DOE, grant No. DE-SC0008712 (primary support) and by the AFOSR, grant No. FA9550-09-1-0230 (partial support).

References

[1] G. Paulavicius, V. Mitin, and M. A. Stroscio, "Hot-optical-phonon effects on electron relaxation in an algaas/gaas quantum cascade laser structure," *Journal of Applied Physics*, vol. 84, no. 7, pp. 3459–3466, 1998.

[2] M. S. Vitiello, R. C. Iotti, F. Rossi, L. Mahler, A. Tredicucci, H. E. Beere, D. A. Ritchie, Q. Hu, and G. Scamarcio, "Non-equilibrium longitudinal and transverse optical phonons in terahertz quantum cascade lasers," *Applied Physics Letters*, vol. 100, no. 9, p. 091101, 2012.

[3] R. C. Iotti, F. Rossi, M. S. Vitiello, G. Scamarcio, L. Mahler, and A. Tredicucci, "Impact of nonequilibrium phonons on the electron dynamics in terahertz quantum cascade lasers," *Applied Physics Letters*, vol. 97, no. 3, p. 033110, 2010.

[4] J. T. Lu and J. C. Cao, "Monte carlo simulation of hot phonon effects in resonant-phonon-assisted terahertz quantum-cascade lasers," *Applied Physics Letters*, vol. 88, no. 6, p. 061119, 2006.

[5] S. Usher and G. P. Srivastava, "Theoretical study of the anharmonic decay of nonequilibrium lo phonons in semiconductor structures," *Phys. Rev. B*, vol. 50, pp. 14 179–14 186, Nov 1994.

[6] H. Page, C. Becker, A. Robertson, G. Glastre, V. Ortiz, and C. Sirtori, "300 K operation of a GaAs-based quantum-cascade laser at $\lambda \approx 9\ \mu m$," *Applied Physics Letters*, vol. 78, no. 22, pp. 3529–3531, 2001.

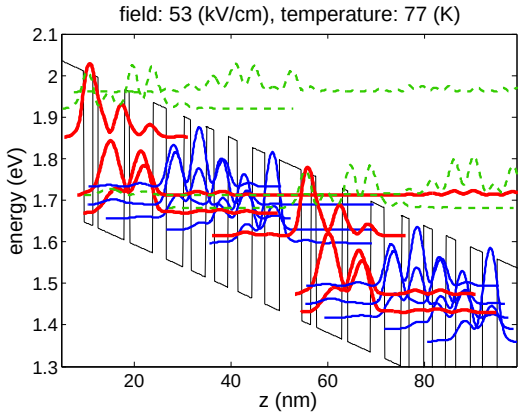

Fig. 1. Energy levels and wavefunction moduli squared of Γ valley subbands in two adjacent stages. The bold red curves denote the upper and lower lasing levels and the ground state in the active region. The blue curves represent injection states and the green curves indicate the Γ continuum-like states.

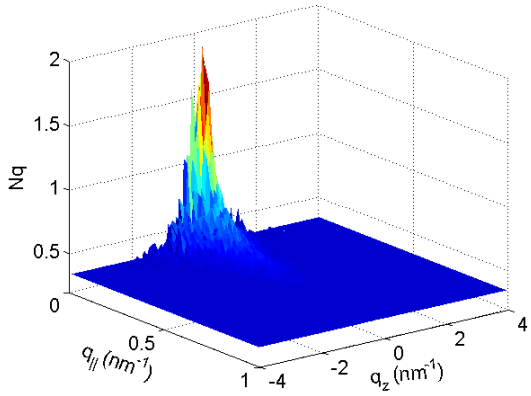

Fig. 2. Nonequilibrium LO phonon occupation number as a function of the in-plane wavevector modulus ($q_{\|}$) and cross-plane wavevector (q_z), for the operating mid-infrared QCL considered in the text.

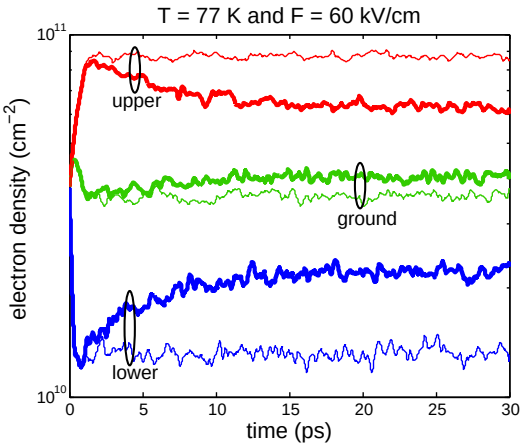

Fig. 3. Time evalution of electron density in upper and lower lasing levels and the ground state in the active region with equilibrium (normal) and nonequilibrium (bold) phonons.

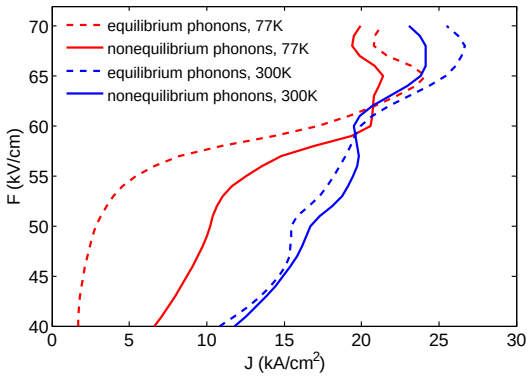

Fig. 4. Current density as a function of applied electric field under different lattice temperatures and conditions for the LO-phonon subsystem: 77 K with equilibrium (red dashed) and nonequilibrium (red solid) phonons, and 300 K with equilibrium (blue dashed) and nonequilibrium (blue solid) phonons.